ELSEVIER

Surface Science 490 (2001) 76–84

SURFACE SCIENCE

www.elsevier.com/locate/susc

Surface charge compensation and ferroelectric domain structure of triglycine sulfate revealed by voltage-modulated scanning force microscopy

V. Likodimos [a,*], M. Labardi [a], M. Allegrini [a], N. Garcia [b], V.V. Osipov [b]

[a] *INFM and Dipartimento di Fisica, Università di Pisa, Via F. Buonarroti 2, I-56127 Pisa, Italy*

[b] *Laboratorio de Fisica de Sistemas Pequeños y Nanotecnologia, CSIC, c/Serrano 144, 28006 Madrid, Spain*

Received 15 January 2001; accepted for publication 25 May 2001

Abstract

The interplay between surface morphology and ferroelectric domain structure on triglycine sulfate (TGS) (0 1 0) cleavage faces is investigated by voltage-modulated scanning force microscopy in the dynamic contact mode. A resonance enhancement method is exploited to increase imaging contrast and sensitivity to slight variations of surface polarity. Evidence of electric contrast of the structural nuclei forming due to surface reconstruction of the TGS cleavage face, is provided, further supported by second harmonic measurements. Lateral growth at ambient conditions and high mobility of the surface nuclei relative to the spontaneous ferroelectric domain motion after cooling from above T_c is detected. Surface charge screening by the conductive liquid film that condenses on the cleavage surface and its interface dynamics are suggested to determine the kinetics of surface nuclei during ferroelectric domain coarsening and the formation of a zig-zag domain boundary.

Keywords: Atomic force microscopy; Surface structure, morphology, roughness, and topography; Surface relaxation and reconstruction; Dielectric phenomena; Single crystal surfaces

1. Introduction

The potential utilization of ferroelectric materials in a wide range of applications as well as the revived interest in fundamental problems related to ferroelectricity has stimulated intensive research exploiting recent advances in microscopic experimental methods. Scanning force microscopy (SFM) offers the possibility to detect and even manipulate polarization domains on ferroelectric surfaces down to the nanoscale range, useful for both practical applications and the study of ferroelectric and related structural phenomena at the submicroscopic scale [1–4].

Among the various SFM techniques, voltage-modulated SFM (VM-SFM), which relies on the electric/electromechanical response to an external modulation voltage [1,5–7], is attracting increasing attention as a very sensitive method to study polarization domains and their dynamics on ferroelectric surfaces [8–21]. A thorough study of the

* Corresponding author. Present address: Institute of Material Science, NCSR Demokritos, 15310 Aghia Paraskevi, Athens, Greece. Tel.: +301-6503381; fax: +301-6511962.

E-mail address: likodimo@ims.demokritos.gr (V. Likodimos).

0039-6028/01/$ - see front matter
PII: S0039-6028(01)01227-4

frequency response in contact mode of VM-SFM and its implications on domain contrast mechanisms has revealed a pronounced resonance effect, which can greatly enhance the force signal and the sensitivity of the method to slight variations of surface polarity [22].

Triglycine sulfate (TGS), whose domain structure has been extensively studied over the last decades [23,24], is a suitable material to explore the capability of SFM to probe its domain and surface morphology [25–36] and to study domain dynamics on the nanoscale [11,18–21,25,26]. TGS undergoes a typical second order phase transition at the Curie temperature $T_c \approx 49°C$, with the vector of spontaneous polarization (P_s) along the *b*-axis. Various 180° domain configurations may form in the ferroelectric phase, the most common being those of rod shape along the *b*-axis with lenticular cross section in the *ac* plane [27].

Selective etching between antiparallel domains on the hygroscopic TGS cleavage surfaces in ambient conditions [28] has been used to differentiate domain polarity. The corresponding surface morphology comprising round holes and islands separated by steps of height $b/2 \approx 0.6$ nm, may arise from dissolution/recrystallization processes taking place in the adsorbed water layer on the crystal surface [25,26]. Although the identification and differentiation of these surface patterns from ferroelectric domains by SFM is far from straightforward [29–31], their structural origin has been verified by topographic and friction force microscopy studies [32–34]. Friction force contrast within and between domains has been analyzed with respect to the different molecular composition of the domain surfaces and asymmetric surface potentials in TGS [35,36]. The time evolution of the round islands has been found to comply with the growth of two-dimensional nuclei in supersaturated solution [37]. Recently, water-assisted surface reconstruction, probed topographically by SFM in conditions of controlled humidity, has been related to the molecular and crystal structure of TGS, surface mass transport and minimization of the total energy of the domain ends [38,39]. However, the role of structural nuclei and surface charge screening in the process of domain coarsening has not been explored.

In this work, we have applied VM-SFM with resonance enhanced contrast, to investigate the relation of surface nuclei to the ferroelectric domain structure on freshly cleaved TGS faces, at ambient conditions. A diverse electric response of surface nuclei compared to that of ferroelectric domains is observed and verified by second harmonic measurements. The instability of the domain interface, giving rise to the formation of a zig-zag boundary, along with the growth and mobility of the surface nuclei with respect to ferroelectric domain kinetics, is also observed and associated with the interface dynamics of the charged surface layer.

2. Experimental method

SFM measurements were performed in the dynamic contact mode using the voltage modulation technique [1]. The method is based on the application of an ac voltage between the conductive tip and the rear sample electrode. Polarization-dependent forces due to the electrostatic tip–surface interaction and the local piezoelectric deformation of the sample modulate the cantilever bending at the excitation frequency, which is detected by means of lock-in techniques [5–7]. The main advantage of VM-SFM is that strong domain contrast can be obtained with no essential correlation with topographic features, which may interfere in the domain images acquired by non-contact or friction SFM measurements [22]. Quantitative analysis of the force signal is difficult due to the competition of electrostatic and electromechanical effects [6,7,11,19], which can vary according to the mechanical response of the cantilever [22] and the particular surface properties including the presence of dielectric screening layers [40]. Recently, we have shown that resonance enhancement in the dynamic contact mode operation of VM-SFM can be achieved by the excitation of resonant modes of the cantilever vibration resulting in a marked amplification of the force signal, despite the constraint imposed on the tip motion in contact conditions [22,41].

Measurements were performed using a home-built SFM that implemented voltage-modulation

[18,19]. Doped silicon cantilevers ($\rho \sim 0.01$ Ωcm) from Nanosensors™, with resonance frequencies of about 15 kHz and nominal spring constants of about 0.1 N/m, were used. Slices (thickness ≈ 0.5–1 mm) of TGS single crystals were cleaved along the (0 1 0) plane, in air, with no further treatment. An ac voltage was applied between the conductive tip and the sample mounted with thermally conducting paste on a flat metallic electrode. The modulation frequency was varied between 10 and 100 kHz, with a peak-to-peak amplitude of 5 V. A dual lock-in amplifier was used to record the amplitude (R) and phase (θ) or the in-phase (X) and out-of phase (Y) components of the normal cantilever oscillations simultaneously with the topographic image. A dithering piezoslab, utilized in the non-contact mode, was used for viscoelastic measurements [22], while thermal treatment and temperature stabilization were carried out using a temperature controller integrated in the microscope head [18].

To optimize detection conditions, the cantilever deflection signal was measured as a function of modulation frequency on the studied TGS specimens. Fig. 1a shows an example of the frequency dependence of the domain contrast function in its real (C_X) and imaginary (C_Y) parts, calculated from the corresponding X and Y components of the ac signal, measured at two positions corresponding to domains of opposite polarity. Contrast enhancement, inversion and nullity can be clearly seen as a function of modulation frequency, in good agreement with our previous results [22, 41]. Fig. 1b shows the frequency variation of contrast amplitude which exhibits a sharp resonance peak centered at 64 kHz (FWHM = 1.5 kHz) that differs significantly from the two resonance peaks, namely at 12.0 and 80.0 kHz, of the freely vibrating cantilever (Fig. 1c). These spectra were measured under the same excitation conditions as in Fig. 1a, but with the tip retracted out of contact. Such behavior can be explained by the excitation of a modified resonance mode of the cantilever, when the tip is in contact conditions [22]. The latter mode is at much higher frequency than the fundamental mode of the free cantilever. Tuning the modulation frequency to the resonance peak in contact conditions provided the enhanced sensitivity, necessary to reveal the finest details of the measurements reported hereafter.

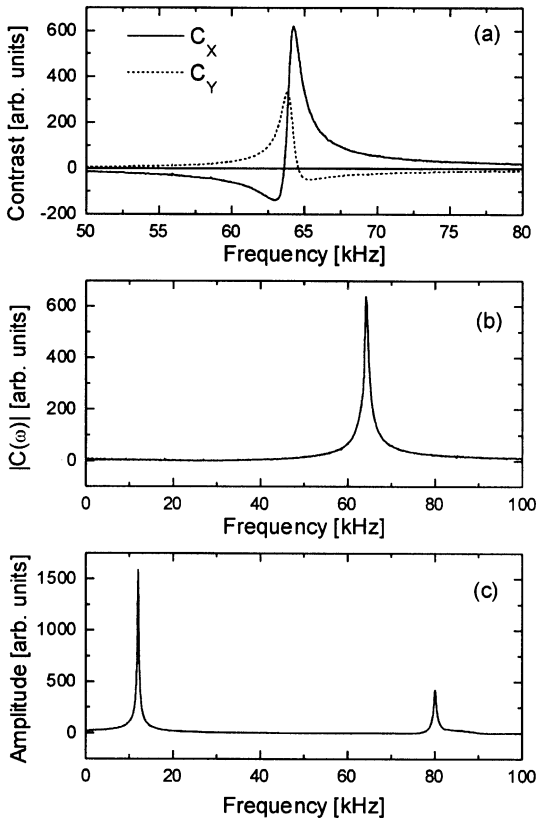

Fig. 1. Frequency spectrum of (a) the real $C_X(\omega) = X(r^+,\omega) - X(r^-,\omega)$ and imaginary $C_X(\omega) = Y(r^+,\omega) - Y(r^-,\omega)$ part of the contrast function $C(\omega) = C_X(\omega) + iC_Y(\omega)$, calculated from the corresponding in-phase (X) and out-of-phase (Y) signal components for two tip positions, r^+ and r^-, within oppositely polarized domains, (b) domain contrast amplitude $|C(\omega)|$ in contact conditions, and (c) amplitude of the ac signal out of contact conditions.

3. Results

3.1. Formation of a zig-zag domain boundary

Fig. 2 shows successive domain images recording the amplitude signal (R) on a cleaved TGS (0 1 0) surface under ambient conditions, 90 min after cleaving the specimen. Scanning over a relatively large sample area revealed an extended

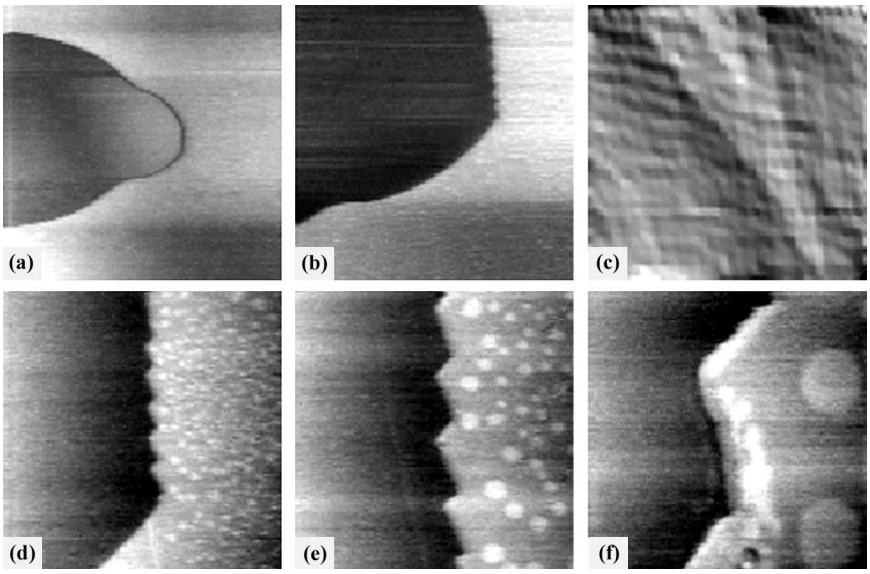

Fig. 2. Domain (R) images at increasing magnifications of a freshly cleaved TGS surface. The images correspond to scan size of (a) 60×60 μm^2, (b) 20×20 μm^2, (c) topography corresponding to the previous image, with z extension range of 6 nm, (d) 9.3×9.3 μm^2, (e) 4.2×4.2 μm^2, (f) 1.5×1.5 μm^2.

domain with distorted lenticular shape embedded in a matrix of opposite polarity, as shown in Fig. 2a. The amplitude on the two oppositely polarized domain areas reveals two different signal levels ($R_+ \neq R_-$), indicating the presence of an intrinsic dc offset voltage, which alters the amplitude of the force signal on the two domain states [41]. The origin of this dc bias can be explained by the contact potential difference at the interface between tip and sample and possibly the presence of different screening conditions of the domain areas, as suggested below. Moreover, the amplitude at the domain boundary appears depleted, in accord with the suppressed force signal at the domain wall [8].

Images of the same area at higher magnification revealed a zig-zag domain boundary at the right-side of the domain wall, which deviates considerably from the pointed ends expected for the usual lenticular domain shape (Fig. 2d–f). The zig-zag wall extends approximately over 6 μm, with a period of about 1 μm, and shows non-uniform contrast (Fig. 2f). The simultaneously acquired topographic images (Fig. 2c) show the saw–tooth steps characteristic of a TGS cleavage surface [30–33]. The cleavage steps can be traced on the domain images by the faint lines most clearly seen in Fig. 2d and e. Such a topographic effect may appear in domain images due to the local distortion of the tip–sample capacitance at the cleavage steps [11].

Zig-zag 180° domain walls have been occasionally reported at much larger spatial scales in the course of switching by sinusoidal fields or in the static domain structure of aged TGS crystals [24]. Their formation might be related to the domain boundary instability induced by the small tilting of 180° domain walls, which in this case become charged, relative to the direction of P_s [24]. At tilting angles exceeding a critical value, the domain boundary may loose its stability under the action of the electric field component due to the bound charge of the domain wall that becomes higher than the coercive field, and transform into the zig-zag form. Apart from differences in the screening conditions of opposite faces of ferroelectric samples, inevitably realized in the tip–sample–electrode configuration, tilting of 180° domain walls may be further enhanced in real crystals by the interaction with defects acting as pinning sites of

the domain walls and causing their static deformation [24].

In this respect, the observation of a stable and distorted domain with substantial necking and the zig-zag shaped wall seems to comply with the stabilization effect of defects and impurities causing the formation of residual domains on TGS crystals and the deformation of the domain boundaries. However, an alternative and meaningful explanation for the peculiar zig-zag domain wall can be suggested in terms of the surface charge screening process by the conductive water layer and its interface dynamics, as will be discussed below (Section 4).

3.2. Formation of surface nuclei

Inspection of the same image series (Fig. 2) shows that numerous round islands exhibiting considerably higher image contrast than that of the cleavage steps, have been progressively resolved on the right-hand domain polarity, while no trace of them could be discerned on the oppositely polarized domain area (Fig. 2d–f). According to etching [28] and SFM studies [29–39], these round islands can be identified with the structural nuclei due to the chemical interaction of the TGS surface layers with the thin water film condensed on the cleavage face, when kept at ambient conditions. This etching process has been found to produce a distinct surface decoration, most pronounced on the positively charged domains (spontaneous polarization P_s pointing out of the sample surface) that etch more strongly due to the increased diffusion rate of positive glycinium ions [28–39].

3.2.1. Linear electric response

The electric contrast of the round nuclei invariably attains the highest value of the total domain contrast in all domain images for this sample. Histogram analysis of the corresponding images (Fig. 2d–f), reveals three distinct R signal levels. The highest one corresponds to the round nuclei ($R_N \approx 66$) and the two lower ones ($R_+ \approx 57$, $R_- \approx 27$) to the opposite domain polarities. Comparison of the former R_N value with the average domain signal, $(R_+ + R_-)/2$, serving as reference background, yields an increase of approximately 20% for the amplitude signal over the round nuclei with respect to that of the domains. A rough approximation of the tip–surface interaction in contact mode of VM-SFM with a simple plate capacitor model, shows that the first harmonic signal stemming from either the piezoelectric or electrostatic effect is proportional to the product of P_s and permittivity of the material [42]. Even though this analysis of the force signal neglects screening effects and the asymmetric electric field distribution in the vicinity of the probe tip, a definite difference between the linear electric response of the surface nuclei and the surrounding domain area can be inferred.

3.2.2. Temporal evolution

Time dependent measurements on freshly cleaved TGS specimens at ambient conditions confirmed the formation of round islands with significant polarization contrast in several cases, even though ferroelectric domain walls were not always detected on the surfaces inspected. Fig. 3 shows examples of such domain images where the R signal at a modulation frequency of 64 kHz, corresponding to the resonance peak in the frequency spectrum of Fig. 1, has been recorded. The domain images 60 and 300 min after cleavage of the specimen (Fig. 3a and b), show that the observed round nuclei grow laterally in accord with a previous topographic SFM study [37]. However, we could not identify the critical radius below

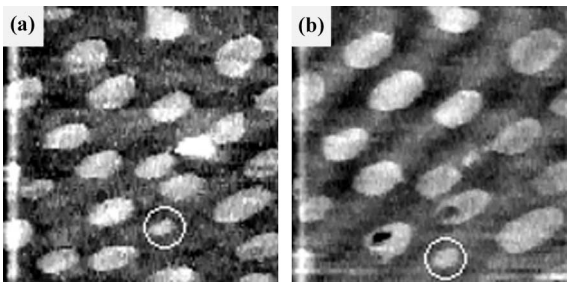

Fig. 3. Domain (R) images of the TGS (0 1 0) surface recorded (a) 60 min and (b) 300 min, after cleavage. The radius of the nuclei enclosed in the dotted circle in (a) is $r \approx 150$ nm. Scan size 4.2×4.2 μm^2.

which the round nuclei shrink and eventually disappear, even for the smaller nucleus ($r \approx 150$ nm) depicted in the imaging frame (Fig. 3).

Measurements on TGS specimens, after prolonged exposure to the atmosphere for several days after cleavage, showed significant etching on ferroelectric domains of both polarities. Fig. 4 shows such an 'aged' TGS surface, exposed to the environment for more than five days after annealing at temperatures above T_c, and several weeks after cleavage. Successive magnifications on the lamellar domain pattern (Fig. 4a), which exhibits strong domain contrast at the resonance frequency, reveals extensive coverage with irregularly shaped etch patterns of both areas corresponding to oppositely polarized domains (Fig. 4b and c).

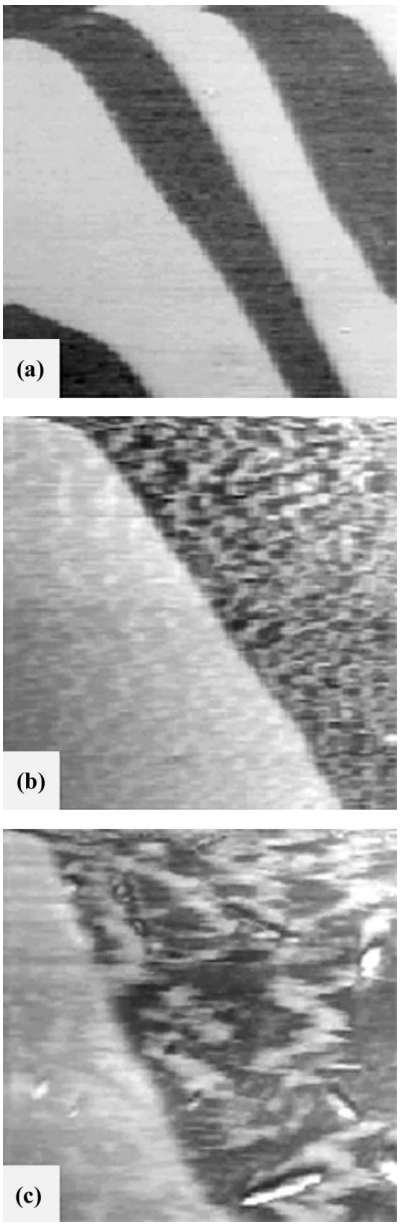

Fig. 4. Domain images of an 'aged' TGS (0 1 0) surface after prolonged exposure to ambient conditions. Scan size (a) 20×20 μm^2, (b) 4.2×4.2 μm^2, and (c) 1.5×1.5 μm^2.

3.2.3. Second harmonic electric response

To explore the origin of the observed nuclei, viscoelasticity and second harmonic VM-SFM measurements were performed on the same surface area that is shown in Fig. 3. Viscoelasticity imaging, using the same excitation frequency of 64 kHz, gave no sign of contrast for the round nuclei, indicating a uniform mechanical response. According to the same approximation of the tip–sample interaction in VM-SFM [5–7], measurements at the second harmonic of the excitation frequency ought to be sensitive to electrostriction and/or permittivity of the sample. If the gap between tip and sample is sufficiently small, as in the present contact mode measurements, the second harmonic signal is proportional to the square of the sample dielectric permittivity, independently of the electric or electromechanical origin of the force signal [42]. To exploit the resonance effect for enhanced second harmonic imaging, measurements were carried out on the same surface area at modulation frequency of 32 kHz, that is half the resonance frequency, and lock-in detection of both first and second harmonics of the ac signal [41]. The second harmonic images exhibit faint contrast of the round nuclei compared with spurious adsorbed surface features characterized by a different dielectric constant. Accordingly, histogram analysis of the R signal in both first and second harmonic images, reveals a rather small contribution of permittivity to the signal for the round nuclei, further supporting an appreciable deviation of their polarization response from the surrounding domain polarity.

3.3. Surface nuclei and domain relaxation

Given the significant domain relaxation in TGS samples after cooling through the ferroelectric phase transition [11,18,21,25], the relative time evolution of surface and domain nuclei was studied on a cleaved TGS specimen. The sample was annealed at 60°C for 60 min and then cooled at a rate of 4°C/min to 24°C. Shortly after thermal equilibration, a relatively coarse domain pattern was detected, which evolved slowly for the first 90 min. Fig. 5 shows the subsequent evolution over 125 min, which was monitored recording the amplitude (R), in-phase (X) and phase (θ) signals. The images reveal relatively large domains, with irregular shaped walls along with the formation of round nuclei with varying lateral dimensions. Slow coarsening of the domain pattern occurs within the first 30 min (Fig. 5a–c). The round nuclei show now a slightly lower polarization signal compared with the surrounding domain area, in the corresponding R images (Fig. 5a, d and g), while their diverse electric response can be clearly discriminated by the intermediate contrast level compared to that of ferroelectric domains on the X and θ images. In most cases, the round nuclei become slightly stretched along the horizontal scan direction. Moreover, the central nucleus B (Fig. 5a), which lies very close to the center of the imaging frame, where the SFM tip rests after each scan, has a much faster rate of lateral growth than the surrounding nuclei.

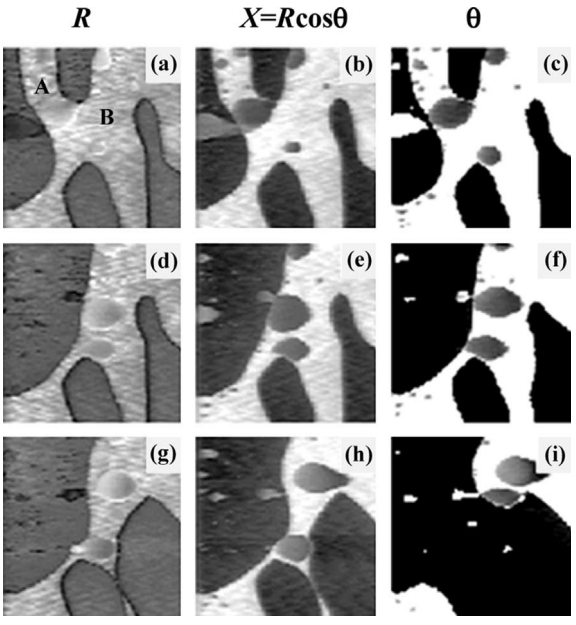

Fig. 5. A sequence of domain images at the TGS (0 1 0) cleavage surface after cooling from 60°C to 24°C. The images are recorded in the amplitude (R), in-phase (X) and phase (θ) signal components, at time intervals of (a) 0 min, (b) 11 min, (c) 30 min, (d) 60 min, (e) 50 min, (f) 75 min, (g) 103 min, (h) 112 min, and (i) 125 min. The offset time after thermal equilibrium at 24°C until the pattern of (a), taken as reference time, is 90 min. Scan size 35×35 μm^2.

Subsequently, domains expand laterally and progressive rounding of their necks occurs through the sideways wall motion at a faster coarsening rate, eventually leading to their coalescence (Fig. 5d–i). In the same time interval, the large surface nuclei A and B show significant mobility, while smaller nuclei seem to be absorbed by the coalesced domains. In particular, the two large nuclei A and B gradually become confined by the growing domains. After domain coalescence, they migrate in order to adjust their position inside the domain area of the same polarity or even to the curvature of the ferroelectric domain boundaries.

4. Discussion

Based on extensive investigations of the structural morphology of these surface nuclei [29–39], their polarity can be, in principle, presumed to be that of the underlying domain area. However, molecules of air, primarily water vapor that condenses on the crystal surface, can essentially modify the surface properties on a freshly cleaved specimen. Relying on the higher solubility rate of a positive domain end [28], dissolution of the corresponding TGS monolayer (comprising positive glycinium and negative sulfate ions) is expected to occur due to the adsorbed water film. The dissolution process would be further accompanied by screening of the surface charge, as the surface water film is a conductive electrolyte. Accordingly, a diverse electric response of the surface nuclei from that of the surrounding domain area may occur,

depending essentially on the modification of the screening conditions of the newly formed nuclei. This explanation complies with the previous suggestion that the observed nuclei may correspond to regions with poor screening of the spontaneous polarization, inferred from the observation of 'erasure' of the corresponding SFM contrast after voltage pulses or local illumination [30].

Assuming that part of the positively charged monolayer on the crystal surface is dissolved by the water film immediately after the cleavage, transportation to other regions including the negatively charged surface may occur with the passage of time. The latter is in accord with the non-uniform domain contrast observed on both domain polarities after prolonged exposure to the atmosphere (Fig. 4). The growth of surface nuclei, the zig-zag shaped domain boundary and the high mobility of surface nuclei relative to the temporal transformation of the ferroelectric domain structure, may then be determined by the interface dynamics of the conductive water film. This process bears close resemblance to the problem of electrodeposition in electrolytic solution and solidification, where interface instabilities may give rise to zig-zag shaped boundaries [43,44]. In this case, the zig-zag domain boundary may form due to the instability of the plane front of the water film growing in the process of electrolysis.

The different dissolution rates of positive and negative domain surfaces and the consequent modification of charge concentration in the corresponding screening layer, may lead to an additional contribution to the dc potential offset deduced from the inequality of the amplitude levels of the VM-SFM signal on oppositely polarized domains. Further, another possible contribution to the surface dynamics due to the probe tip influence [32,45] might be inferred from the distortion of the nuclei's shape along the scan direction and the relatively high rate of lateral growth of nucleus *B* in Fig. 5. Even though we have not observed polarization switching below the tip, it is possible that the high electric field density on the apex of the conductive tip [17] might cause redistribution of the screening charges when acting for sufficient time over the same local area, and thus promote the mobility of surface nuclei.

5. Conclusions

Resonance enhancement of sensitivity in voltage-modulated SFM operated in the dynamic contact mode, provides a very effective method to investigate the surface morphology and its electric response relative to the static and dynamic ferroelectric domain structure of cleaved TGS surfaces. Round structural nuclei, due to the water-assisted reconstruction of the TGS cleavage surface at ambient conditions, exhibit different electric contrast with respect to that of oppositely polarized domains. This effect has been associated with the different screening conditions induced by the conductive water film. The formation of a zig-zag domain boundary, the growth and mobility of the surface nuclei occurring during the coarsening of the ferroelectric domain structure, has been related to the interface dynamics of the conductive water layer.

Acknowledgements

We gratefully acknowledge EC for financial support within the TMR Network ERBFMR-XCT98-024. One of us (V.V.O) thanks the Spanish sabbatical program for financial support. We wish to thank the referees for very helpful comments and suggestions.

References

[1] F. Saurenbach, B.D. Terris, Appl. Phys. Lett. 56 (1990) 1703.
[2] R. Lüthi, H. Haefke, P. Grütter, L. Szczesniak, H.-J. Güntherodt, K.-P. Meyer, Surf. Sci. Lett. 285 (1993) L498.
[3] R. Lüthi, H. Haefke, K.-P. Meyer, E. Meyer, L. Howald, H.-J. Güntherodt, J. Appl. Phys. 74 (1993) 7461.
[4] O. Kolosov, A. Gruverman, J. Hatano, K. Takahashi, H. Tokumoto, Phys. Rev. Lett. 74 (1995) 4309.
[5] K. Franke, J. Besold, W. Haessler, C. Seegebarth, Surf. Sci. Lett. 302 (1994) L283.
[6] K. Franke, Ferroelectric Lett. Sect. 19 (1995) 25.
[7] K. Franke, M. Weihnacht, Ferroelectric Lett. Sect. 19 (1995) 35.
[8] J. Ohgami, Y. Sugawara, S. Morita, E. Nakamura, T. Ozaki, Jpn. J. Appl. Phys. Part 1 35 (1996) 2734.

[9] M. Abplanalp, L.M. Eng, P. Günther, Appl. Phys. A 66 (1998) S231.
[10] L.M. Eng, H.-J. Güntherodt, G. Rosenman, A. Skliar, M. Oron, M. Katz, D. Eger, J. Appl. Phys. 83 (1998) 5973.
[11] J.W. Hong, K.H. Noh, S.-I. Park, S.I. Kwun, Z.G. Khim, Phys. Rev. B 58 (1998) 5078.
[12] T. Hidaka, T. Maruyama, M. Saitoh, N. Mikoshiba, M. Shimizu, T. Shiosaki, L.A. Wills, R. Hiskes, S.A. Diracolis, J. Amano, Appl. Phys. Lett. 68 (1996) 2358.
[13] A. Gruverman, O. Auciello, H. Tokumoto, Appl. Phys. Lett. 69 (1996) 3191.
[14] G. Zavala, J.H. Fendler, S.T. McKinstry, J. Appl. Phys. 81 (1997) 7480.
[15] T. Tybell, C.H. Ahn, J.-M. Triscone, Appl. Phys. Lett. 72 (1998) 1454.
[16] K. Franke, H. Huelz, M. Weihnacht, Surf. Sci. 416 (1998) 59.
[17] C. Durkan, M.E. Welland, D.P. Chu, P. Migliorato, Phys. Rev. B 60 (1999) 16198.
[18] V. Likodimos, X.K. Orlik, L. Pardi, M. Labardi, M. Allegrini, J. Appl. Phys. 87 (2000) 443.
[19] X.K. Orlik, V. Likodimos, L. Pardi, M. Labardi, M. Allegrini, Appl. Phys. Lett. 76 (2000) 1321.
[20] E.Z. Luo, Z. Xie, J.B. Xu, I.H. Wilson, L.H. Zhao, Phys. Rev. B 61 (2000) 203.
[21] V. Likodimos, M. Labardi, M. Allegrini, Phys. Rev. B 61 (2000) 14440.
[22] M. Labardi, V. Likodimos, M. Allegrini, Phys. Rev. B 61 (2000) 14390.
[23] M.E. Lines, A.M. Glass, Principles and Applications of Ferroelectrics and Related Materials, Clarendon, Oxford, 1977.
[24] L.I. Dontsova, N.A. Tikhomirova, L.A. Shuvalov, Kristallografiya 39 (1994) 158 (Crystallography Reports 39 (1994) 140).
[25] R. Lüthi, H. Haefke, W. Gutmannsbauer, E. Meyer, L. Howald, H.-J. Güntherodt, J. Vac. Sci. Technol. B 12 (1994) 2451.
[26] H. Haefke, R. Lüthi, K.-P. Meyer, H.-J. Güntherodt, Ferroelectrics 151 (1994) 143.
[27] K. Takahashi, M. Takagi, J. Phys. Soc. Jpn. 44 (1978) 1266.
[28] A. Sawada, R. Abe, Jpn. J. Appl. Phys. 6 (1967) 699.
[29] A. Correia, J. Massanell, N. Garcia, A.P. Levanyuk, A. Zlatkin, J. Przeslawski, Appl. Phys. Lett. 68 (1996) 2796.
[30] N. Garcia, A.P. Levanyuk, J. Massanell, J. Przeslawski, A. Zlatkin, J.L. Costa, Ferroelectrics 184 (1996) 1.
[31] L.M. Eng, J. Fousek, P. Günther, Ferroelectrics 191 (1997) 211.
[32] H. Bluhm, R. Wiesendanger, K.-P. Meyer, J. Vac. Sci. Technol. B 14 (1996) 1180.
[33] H. Bluhm, K.-P. Meyer, R. Wiesendanger, Ferroelectrics 200 (1997) 327.
[34] L.M. Eng, M. Bammerlin, Ch. Loppacher, M. Guggisberg, R. Bennewitz, R. Luthi, E. Meyer, H.-J. Güntherodt, Appl. Surf. Sci. 140 (1999) 253.
[35] H. Bluhm, U.D. Schwarz, K.-P. Meyer, R. Wiesendanger, Appl. Phys. A 61 (1995) 525.
[36] H. Bluhm, U.D. Schwarz, R. Wiesendanger, Phys. Rev. B 57 (1998) 161.
[37] J. Ohgami, Y. Sugawara, S. Morita, T. Ozaki, J. Phys. Soc. Jpn. 66 (1997) 2747.
[38] S. Balakumar, J.B. Xu, G. Arunmozhi, R. Jayavel, N. Nakatani, T. Yamazaki, Jpn. J. Appl. Phys. 37 (1998) 6177.
[39] S. Balakumar, H.C. Zeng, J. Mater. Chem. 10 (2000) 651.
[40] S.V. Kalinin, D.A. Bonnell, Appl. Phys. Lett. 78 (2001) 78.
[41] M. Labardi, V. Likodimos, M. Allegrini, Appl. Phys. A 72 (2001) S79.
[42] K. Franke, H. Huelz, M. Weihnacht, Surf. Sci. 415 (1998) 178.
[43] D. Bensimon, Phys. Rev. A 33 (1986) 1302.
[44] V.V. Gafiichuk, I.A. Lubashevskii, V.V. Osipov, Dynamics of Formation of Surface Structures in Systems with Free Boundary, Naukova Dumka, Kiev, 1990.
[45] A.L. Tolstikhina, N.V. Belugina, S.A. Shikin, Ultramicroscopy 82 (2000) 149.